Mon. Not. R. Astron. Soc. **336,** 197–206 (2002)

Classification of a selected sample of weak T Tauri stars

J. Gregorio-Hetem[1]★ and A. Hetem, Jr[2]★

[1] *Universidade de São Paulo, IAG/USP, Rua do Matão 1226, 05508-900 São Paulo, SP, Brazil*
[2] *Universidade Paulista, UNIP/ICET, Rua Dr Bacelar 1212, 04026-002 São Paulo, SP, Brazil*

Accepted 2002 May 28. Received 2002 May 27; in original form 2002 January 16

ABSTRACT

We studied a sample of 27 T Tauri stars (TTs) showing a weak Hα line, selected from the *Pico dos Dias* Survey, a search for young stellar objects. A model to fit the spectral energy distribution is used in order to reproduce their observed infrared excess and to evaluate the individual contribution of the circumstellar components (dust disc and/or envelope) to the total emitted flux. The objects were separated into different categories of young stars, searching for an agreement with an evolutionary sequence. The classification is based on the stellar characteristics as spectral type; equivalent width of the Li 670.8-nm line; optical and X-ray properties; and infrared excess. We conclude that only 41 per cent of our sample actually correspond to weak TTs, and the remaining objects are mainly classical TTs or young main-sequence stars. Most of the stars have a near-infrared index typical of Class II objects and show an important fraction of the observed emission ($\sim$30 per cent) being generated by the circumstellar material.

Key words: circumstellar matter – stars: fundamental parameters – stars: pre-main-sequence – infrared: stars.

1 INTRODUCTION

The motivation in classifying the weak T Tauri stars (WTTs), often called 'naked' TTs, has mostly arisen after the discovery of several possible WTTs located far from molecular clouds, detected by the *ROSAT* All-sky Survey (Alcalá et al. 1995; Neuhäuser et al. 1995a,b). Some authors argue that all of these candidates could not be WTTs, but would rather be post TTs or young main-sequence (YMS) stars (e.g. Briceño et al. 1997). The actual evolutionary status of the objects showing X-ray emission typical of pre-main-sequence low-mass stars was discussed by Martín (1997), who presented quantitative spectroscopic criteria searching to clarify the nature of these young stellar objects (YSOs). The same criteria were used to classify a sample of *ROSAT* sources detected in the ρ Oph region (Martín et al. 1998). Their study, on regions showing different molecular cloud properties, revealed different ratios of WTTs to classical T Tauri stars (CTTs), leading to an investigation of the star formation rate in this molecular cloud complex.

Other YSO classification schemes, based on infrared (IR) excess, were proposed earlier than the debate on evolutive status of X-ray candidates. *IRAS* colours have been suggested by several authors as criteria to select YSO candidates (Beichman 1986; Gregorio-Hetem, Sanzovo & Lépine 1988; Harris, Clegg & Haghes 1988), allowing the discovery of both WTTs and CTTs (Gregorio-Hetem et al. 1992; Torres et al. 1995). Weintraub (1990) studied a large sample of *IRAS* sources associated with YSOs from the Herbig & Bell Catalogue (1988, hereafter HBC). Four subclasses of emission-line stars were plotted on *IRAS* spectral slope diagrams, separated into CTT, WTT, Herbig Ae/Be and FU Orionis stars. The position of the WTTs, on these diagrams, is quite coincident with the CTTs *locus*, but restricted to more constrained ranges of *IRAS* flux ratios between wavelengths of 25 and 60 μm. The contribution of the circumstellar matter to the spectral energy distribution (SED) slope is often used to recognize different categories of young objects by following an observational classification based on the spectral index $a \equiv \mathrm{d}(\log \lambda F_\lambda)/\mathrm{d}(\log \lambda)$, calculated in the near-IR range (Lada & Wilking 1984; Wilking, Lada & Young 1989, hereafter WLY89; André et al. 1993). In a study of the 1.3-mm continuum emission of the circumstellar material of 100 YSOs, André & Montmerle (1994) revised the IR classification of WLY89. They suggested a new threshold, $a < -1.5$, better representing the boundary between Class III and Class II sources.

We are interested in classifying the TTs detected in the *Pico dos Dias* Survey (PDS) by Gregorio-Hetem et al. (1992, PDS I hereafter), and Torres et al. (1995, PDS II hereafter). Among several interesting YSOs, this survey has revealed 71 TTs, 39 of them being WTTs (Torres 1998). Some previously known TTs were also included in the PDS observations. We selected the WTTs from the published PDS lists, by adopting the commonly used criterion of Hα equivalent width $W_{\mathrm{H}\alpha} < 10$ Å, a criterion for distinguishing WTTs from the CTTs (Appenzeller & Mundt 1989). Our goal is to reproduce the SED synthetically in order to evaluate the individual contributions from different circumstellar components to the total

★E-mail: jane@astro.iag.usp.br (JG-H); annibal.hetem.jr@usa.net (AH)

emission, to be compared with a spectroscopic classification and other optical, IR and X-ray characteristics. The obtained correlations are used to better classify the programme stars.

The following sections describe the sample selection, the SED fitting model, the classification obtained from the spectroscopic analysis and the IR excess analysis. Finally, a discussion of the results and the conclusions are presented. The last section is an Appendix, dedicated to describing the parameter estimation method used in the adopted model.

2 THE PROGRAMME STARS

The PDS candidates were selected among the southern ($\delta < +30^\circ$) *IRAS* sources having flux ratios in the ranges $0.95 < F_{25}/F_{12} < 3.4$ and $0.60 < F_{60}/F_{25} < 3.3$, where F_λ corresponds to the flux at $\lambda = 12$, 25 or 60 μm.

The nature of the PDS candidates was investigated by means of photometric *UBVRI* observations and medium-resolution spectra, looking for Hα emission and the presence of the Li 670.8-nm line to identify 'new' TTs, not listed in the HBC.

PDS I and PDS II have published data for 29 'new' WTTs, but some of them were not included in our sample as we did not have all the data needed for the calculations of SED fits. This is the case for the binaries PDS047, PDS050 and PDS082, for which individual photometry was not made for each component, and PDS01, PDS045 and PDS055, which are not *IRAS* sources.

Other previously known WTTs (PDS039, PDS053, PDS073 and PDS093) that fill the above criteria were included in the final sample, which contains 27 stars. All of them have optical and far-IR observational data points in their SED, known spectral type and available equivalent widths of Hα and Li 670.8 nm. Basically, the observational data consists of the *UBVRI* photometry and the spectral types obtained in the PDS (updated results were presented by Torres 1998). The effective temperatures were determined by using the conversion of spectral type presented by de Jager & Nieuwenhuijzen (1987). The *IRAS* data were extracted from the Point Source Catalogue. For the previously known objects listed in the HBC we used the co-added *IRAS* fluxes presented by Weaver & Jones (1992). For most of the stars located in the direction of clouds, only an upper limit of the 100-μm *IRAS* flux is available. In order to avoid source/background confusion, only good-quality flux measurements were used in the calculations.

Table 1 lists the stars of our sample by giving the PDS number, *IRAS* identification, spectral type, equivalent width of Hα and Li 670.8 nm lines and the *UBVRI* photometry. Additional information obtained from the public catalogues are also listed: *JHK 2MASS* photometry and X-ray emission (in terms of count rate) and identification of *ROSAT* sources.

3 THE CIRCUMSTELLAR STRUCTURE

3.1 Disc/envelope models

The contribution of the circumstellar dust to the emitted radiation of young stellar systems is mainly evaluated by means of the IR excess observed in these objects. The different hypothesis to explain the configuration of the dust distribution around low-mass YSOs has lead to two basic lines in building models for the circumstellar structure. In one of them it is assumed that the central object is surrounded by a spherical dust envelope and in the other one the presence of a disc orbiting the star is considered. In principle, the IR excess may be produced by an envelope or a disc and the option for one or other model will depend on the evolutionary status of different objects.

Among the different models to reproduce the SED of TTs, we mention here only those more adequate to our programme stars that do not show large amounts of IR excess and are probably more evolved TTs. In the simplest scenario, the TT disc is passive and re-radiates the energy absorbed from the central star. In this case the excess of infrared emission will arise even in the absence of any accretion luminosity (Adams, Lada & Shu 1987; Kenyon & Hartmann 1987; Strom, Edwards & Strutskie 1993). An alternative to the accreting or flared discs models is to consider the addition of a second component to the circumstellar structure: a tenuous dust envelope surrounding the star and the disc that could explain the flattened SED exhibited by most of TTs.

Natta (1993) proposed a three-component model to represent the structure of the TTs. In this model, the system is formed by a star, its circumstellar disc and a dust envelope surrounding both, which scatters stellar radiation back on to the disc. The presence of two circumstellar components is also considered by Calvet et al. (1994), where the flat SED of TTs can be explained by radiative emission from infalling dusty envelopes. In this case, the stellar radiation is absorbed and re-emitted in the IR by the envelope. More recently, Chiang & Goldreich (1997) derived hydrostatic, radiative equilibrium models for passive, reprocessing discs surrounding TTs. In a study of the vertical structure of TT discs, D'Alessio et al. (1999) considered the case of a disc irradiated by the central star. The grains in the surface of the disc are directly exposed to the radiation from the star and the interior of the disc is heated by diffusion from the surface. The SED calculations by Chiang & Goldreich (1997) of passive discs viewed face-on were improved to consider arbitrary inclinations and also to include details on the dust grain proprieties (Chiang & Goldreich 1999; Chiang et al. 2001, respectively). The flat radiative equilibrium disc model is in agreement with the SED presented by our sample in the near-IR range, but the far-IR excess, although small, could not be successfully reproduced. In this case, the presence of a thin dusty envelope could better explain the emission at longer IR wavelengths.

3.2 Model assumptions

In order to reproduce the SED of TTs synthetically, Gregorio-Hetem, Lépine & Ortiz (1990, 1991) used a simple model of a system composed by a central star surrounded by a dust envelope. This model was improved by assuming the presence of a geometrically thin and optically thick passive disc placed between the central star and the envelope. Some preliminary results were obtained for a large sample of TTs (Hetem, Gregorio-Hetem & Lépine 1994). For the selected sample in the present work, the observed SED is well reproduced by this model, where the assumptions are consistent with the flat radiative equilibrium disc model presented by Chiang & Goldreich (1997). The adopted circumstellar structure is displayed in Fig. 1, showing the central star surrounded by an extended and flat disc, and both are enveloped by a thin dust shell. The inner radius of the disc is constrained by an adopted grain destruction temperature and the outer disc radius defines the inner radius of the envelope. The observed data cover the wavelength range of 0.3–100 μm (only PDS039 has 1300-mm emission measured by Henning et al. 1993) and the method finds the best fit by varying the following parameters: radius R_s of the star, radius R_d and inclination angle θ of the disc and radius R_e and optical depth τ_λ of the envelope. Another parameter of the model is the stellar temperature T_s, which is not variable and was estimated from the calibration between spectral type and

Table 1. List of the programme stars and their *IRAS* identification. Spectral type, equivalent width of Hα and lithium lines, and *UBVRI* photometry were obtained from the PDS catalogue. *J*, *H* and *K* magnitudes are from *2MASS* catalogue. The final columns display the X-ray count rate and identification of sources coincident with PDS objects found in the *ROSAT* public archives.

PDS	*IRAS*	S.T.	$W_{H\alpha}$	W_{Li}	*U*	*B*	*V*	*R*	*I*	*J*	*H*	*K*	Cnt/Ks	2RXPJ
030	08131−4432	F7	−2.3	0.13	11.41	11.33	10.73	10.37	10.02					
035	10001−5857	F8	−8.0	0.13	10.63	10.35	9.73	9.27	8.78					
039	10570−7701	K0	−8.0	0.28	13.90	12.95	11.71	10.92	10.10	9.25	8.29	7.72	11.5	105820.8−771700
051	11091−7716	K0	−3.0	0.35		16.22	14.31	12.93	11.67				8.3 ± 0.6	111036.7−773239
053	11108−7620	K2	−2.0	0.31	13.46	12.63	11.52	10.86	10.19	9.42	8.63	8.17	81 ± 18	111233.7−763705
054	11195−2430	K5	−0.1	0.37	11.23	10.14	8.90	8.13	7.39	6.41	5.76	5.58	656 ± 46	112205.4−244632
059	11472−7834	M0	−5.0	0.54	15.39	14.40	12.90	11.86	10.73				101 ± 14	114927.3−785059
064	12535−7623	M0	−3.0	0.29		17.23	15.03	13.49	12.02					
070	14050−4109	K5	−2.0	0.46	14.32	13.45	12.15	11.35	10.58				89 ± 24	140809.8−412352
073	15420−3408	K2	−5.0	0.33	12.60	11.68	10.40	9.64	8.88	7.56	6.84	6.45	137 ± 20	154513.6−341733
077	15573−4147	K0	−2.0	0.32	13.43	12.72	11.60	10.93	10.25					
081	16112−1930	K2	−0.7	0.34	13.78	13.02	11.83	11.09	10.38				184 ± 51	161410.4−193928
083	16225−2607	K7	−10.0	0.40	13.82	12.98	11.68	10.86	10.03	8.70	7.95	7.52	49 ± 13	162538.1−261353
087	16424−2457	K2	−9.0	0.50	12.85	12.15	11.05	10.39	9.76	8.76	8.01	7.68	63 ± 16	164527.9−250319
089	16443−1509	K7	−2.2	0.55	14.66	13.46	12.02	11.12	10.20				83 ± 16	164713.0−151430
093	16514−3648	F5	−3.0	0.01	9.61	9.44	8.82	8.46	8.11					
099	19063−3709	K0	−5.0	0.35	15.82	14.92	13.30	12.26	11.26					
109	05206+0052	F7	2.0V	0.11	10.82	10.78	10.24	9.93	9.62				5.7 ± 1.2	052312.5+005449
110	05209−0107	F5	−6.0	0.08	11.02	10.95	10.42	10.10	9.77	9.18	8.44	7.84		
111	05222−0844	G3	−2.0V	0.26	10.86	10.62	9.88	9.45	9.04	8.38	8.05	7.89	127 ± 18	052437.4−084200
115	05256+0107	G5	−9.0	0.13	11.97	11.73	10.96	10.51	10.06				45 ± 11	052818.6+011007
116	05281+0257	G5	0.5	0.26	11.79	11.48	10.68	10.21	9.76				122 ± 18	053048.3+025932
118	05350−0210	F6	−7.0	0.06	10.58	10.48	9.91	9.56	9.22	8.70	8.16	7.58		
119	05357−0217	F5	−2.0	0.15	11.11	11.02	10.48	10.15	9.84	9.41	9.09	8.90	4.5 ± 1.5	053814.0−021553
138	11507−6148	M6	−0.3	0.60		16.90	14.5	11.7	9.28				18.5	115310.0−620723
145	16114−1858	K7	−1.9	0.20		15.76	13.95	12.78	11.64				6.0 ± 0.9	161420.4−190625
156	18247−0436	G0	−7.0	0.09	13.09	12.48	11.22	10.42	9.64					

Notes: The main-sequence spectral class has been adopted for this sample, but PDS138 has features of a M6III star. The negative values of $W_{H\alpha}$ denote an emission line, and 'V' is used to indicate a variable Hα profile (PDS109 and PDS111).

effective temperature (T_{eff}) proposed by de Jager & Nieuwenhuijzen (1987) for main-sequence stars.

The emission from the star and from the disc are attenuated by the opacity of the envelope and the luminosity contribution of the disc depends on the inclination angle of the system. The flux is calculated by assuming blackbody emission and different temperature laws for the disc and the envelope. The total radiation emitted, as a function of wavelength λ, is the sum of the contributions of each component: $S_s(\lambda)$ of the star, $S_d(\lambda)$ of the disc and $S_e(\lambda)$ of the envelope.

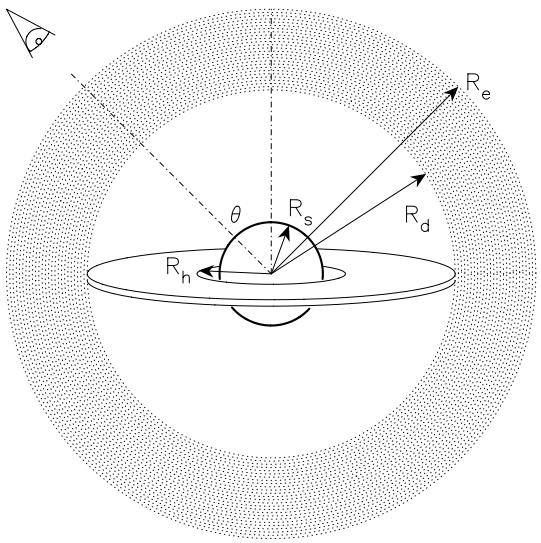

Figure 1. The schematic representation of the model components (the sizes are not to scale).

The absorption and the emission of radiation depend on the total optical depth of the envelope, which is a parameter of the model. The optical depth as a function of the wavelength is given by $\tau_\lambda = \tau_{1\,\mu m} C_{abs}(\lambda)$, where the extinction law is normalized to $C_{abs}(1\ \mu m) = 1$.

We adopted the extinction law $C_{abs}(\lambda)$ obtained by Ossenkopf (1993) from an evolutionary model for fluffy aggregates. Among the models proposed by Ossenkopf, we choose the $C_{abs}(\lambda)$ given by the calculation where the grains evolved during 10^5 yr in a medium with $10^5 < n_H < 10^8$ cm^{-3} and $T < 20$ K that are the physical conditions more consistent with those found in typical star-forming regions. The results given by the adopted opacity law are in agreement with those obtained in other works (e.g. Rowan-Robinson 1986; and by Désert, Boulanger & Puget 1990).

The star is considered here as a spherical blackbody emitter and the flux density is given by

$$S_s(\lambda) = \frac{R_s^2}{d^2} \pi B(\lambda, T_s) e^{-\tau(\lambda)}. \quad (1)$$

The distance d is not known for the whole sample. As we are not attempting to estimate stellar luminosity, a generic value $d = 100$ pc has been adopted.

In this model the disc is assumed to be passive, optically thick and geometrically thin. The total thermal radiation of the disc is

evaluated by assuming that it is composed of several rings with mean radius r_{d_i} and width δr_{d_i}, each one emitting as a blackbody with a temperature law following Adams & Shu (1986):

$$T_{d_i} = T_s \left(\frac{2}{3\pi}\right)^{1/4} \left(\frac{r_{d_i}}{R_s}\right)^{-3/4}. \quad (2)$$

The inner radius of the disc is defined by $R_h = R_s(T_g/T_s)^{-4/3}$, where we adopted $T_g = 1500$ K as the destruction temperature of the grains, by considering the silicate sublimation temperature (Chiang et al. 2001). The viewing angle θ determines the amount of energy detected by the observer, and is maximized when the system is seen 'face-on'. As in the case of the star, the disc emission is attenuated by the opacity of the envelope. The disc contribution to the total emitted flux is obtained by integrating the individual emission of each ring, given by

$$S_{d_i}(\lambda) = \frac{2r_{d_i}\delta r_{d_i}}{d^2} \pi B(\lambda, T_{d_i}) e^{-\tau(\lambda)} \cos\theta. \quad (3)$$

In the integration r_{d_i} varies between R_h and R_d. For the emission from the dust envelope our numerical simulations are based on the radiative transfer model used by Epchtein, Le Bertre & Lépine (1990) to reproduce the IR data of carbon stars. In their model it is assumed that the star is surrounded by a spherically symmetric dust envelope with inner radius defined by the energy balance in the dust grains. The envelope is divided into concentric layers, or spherical shells, each individual shell emitting as a blackbody following the temperature law:

$$T_{e_i} = T_s \left(\frac{2r_{e_i}}{R_s}\right)^{-0.4}. \quad (4)$$

This temperature distribution is in agreement with the classical models used to reproduce the emission of a spherically symmetric distribution of dust, illuminated by a star at the centre, which sits in a spherical dust-free cavity (Rowan-Robinson 1980).

The optical depth at 1 μm is calculated for each shell of the envelope as a function of the density distribution $\tau_i \propto \rho(r)$, where $\rho(r) \propto r^{-3/2}$. The total optical depth integrated between R_d and R_e gives the parameter $\tau_{1\,\mu m}$ of the model. The optical depths at other wavelengths are obtained from the above-mentioned extinction law. The emission of each shell depends on its own optical depth $\tau_i(\lambda)$ and also on the absorption of the remaining shells $\tau_{ext_i}(\lambda)$. The total flux emitted by the envelope is obtained by integrating the individual contributions:

$$S_{e_i}(\lambda) = \frac{r_{e_i}^2}{d^2} \pi B(\lambda, T_{e_i}) e^{-\tau_i(\lambda)} \left[1 - e^{-\tau_{ext_i}(\lambda)}\right]. \quad (5)$$

3.3 The parameter estimation method

The strategy for the *n*-parameter estimation is provided by maximum-likelihood statistics. The goodness-of-fit function is given by the traditional χ^2 statistic assuming the Levenberg–Marquardt method (Press et al. 1992).

The adopted strategy is to fit the parameters in four steps. A first fit is made by considering only the optical band, which is directly affected by T_s, R_s and τ (see equation 1). Then, the near-IR band is used to determine the disc parameters (equation 3). A third fit is made with *IRAS* and millimetric (when available) bands to determine the last parameter, R_e. A final fit is made with all data points for the whole set of initial parameters. This procedure enhances the calculation speed since the code is not 'trapped' in unwanted minima in the χ^2 function and reduces the number of free parameters (in each step).

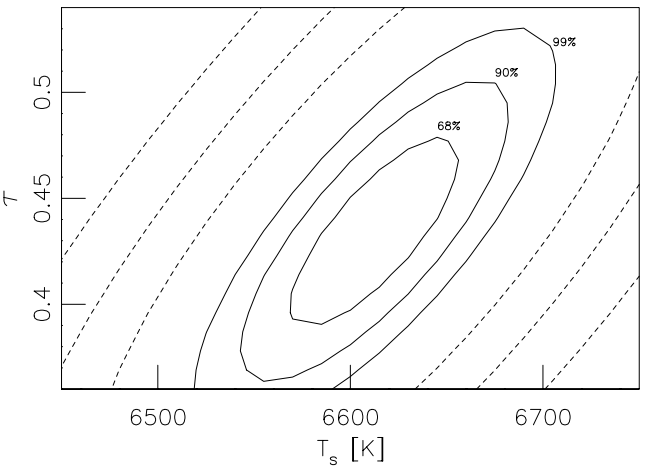

Figure 2. The confidence level in parameter space. In this example we plot the confidence limits for the parameters T_s and τ evaluated for PDS118.

Thamm, Stinacker & Henning (1994) studied the dust disc parametrized models for young stellar objects and discussed the parameter ambiguities. The main problem is that the parameters are weakly constrained in the model, considering the possibility of the data points fitting with different sets of parameters. An example is presented by Bouvier & Bertout (1992) who tried to fit the observed SED of DF Tau and found several ambiguous solutions in their six-parameter disc model.

We estimate the quality of our fitting procedure by considering confidence levels for the fitting parameters. The dependence of two parameters and their confidence limits is demonstrated for PDS118 as an example. Fig. 2 presents the contour levels for the $\chi^2 = f(T_s, \tau)$ surface, where confidence levels for 68, 90 and 99 per cent are indicated. One can see that there is a correlation between T_s and τ, owing to the deviation of the main axis of the ellipses from the orthogonal axes.

3.4 Results of the SED fit

The fitting method looks for the parameter set (R_s, R_d, R_e, τ, θ) providing a solution for the model equations that reproduces the observational data. Actually, the number of free parameters is reduced since the spectral type and the observed $E(B-V)$ give us the estimation of T_s, R_s and τ. The initial values of the other parameters are chosen among those typical of young stars ($R_d = 100$ au, $R_e = 1000$ au, $\theta = 45°$), avoiding unwanted minima and speeding up the code significantly. In order to test the variation in goodness of fit (gof) owing to possible changes in T_s, after obtaining the best fit with T_{eff}, we performed the calculations setting the temperature as a free parameter. A maximum deviation of 150 K was found and in most of the cases the temperature obtained with the SED fit is quite close to the temperature estimated using the calibration T_{eff} versus spectral type.

The optical depth τ obtained from the SED fit was compared with the values derived from the total visual extinction, by using the colour excess $E(B-V)$ measured as described in Section 4.3 and adopting the relations $A_V = 3.1E(B-V)$ and $A_\lambda = 1.086\tau/\lambda$, where λ is given in micrometres. A good correlation was found between the theoretical optical depth and the value obtained as a SED fitting parameter, in spite of the errors that are introduced

Table 2. Stellar parameters obtained with the SED fit; individual contribution of circumstellar components indicated by F_d (disc) and F_e (envelope); type denotes the classification of the programme stars; *UBV* colours corrected for extinction; near-IR spectral index (a_{IR}); far-IR colours; and the X-ray-to-optical flux ratio given by $\log(f_X/f_V)$.

PDS	T_{eff} (K)	R_s ($R_\odot$)	R_d (au)	R_e (au)	τ	θ (deg)	gof	F_d (per cent)	F_e (per cent)	Type	$U-B$	$B-V$	a_{IR}	[12–25]	[25–60]	$\log(f_X/f_V)$
30	6383	1.44	22	1.6E+02	0.68	16	0.009	22	11	YMS	0.04	0.54	−0.7	2.44	1.57	
35	6310	2.87	36	5.9E+04	0.85	0	0.031	18	38	CTT	0.13	0.41	−0.4	2.56	2.48	
39	5039	2.70	187	5.5E+02	1.40	76	0.155	11	18	CTT	0.61	0.75	−1.0	3.38	2.94	−2.4
51	5166	1.19	42	4.4E+01	2.06	48	0.033	39	2	WTT		0.72	−0.4	2.01	1.47	−1.5
53	4836	1.62	0.1	8.8E+02	0.55	0	0.044	17	15	WTT	0.67	0.87	−0.7	1.28	0.72	−1.6
54	4406	5.58	66	4.2E+02	0.69	80	0.071	6	7	PTT	0.96	1.04	−1.3	3.24	1.62	−1.7
59	3837	1.56	4	5.3E+04	0.74	43	0.035	20	20	WTT	0.82	1.25	−0.6	2.84	1.70	−0.9
64	3917	4.07	22	2.3E+01	2.56	70	0.015	28	2	PTT		1.38	−0.4	1.73	1.07	
70	4406	1.39	614	4.5E+03	0.78	0	0.012	29	5	WTT	0.71	1.06	−0.7	2.06	2.70	−1.3
73	4954	4.04	173	5.7E+02	0.98	0	0.023	30	8	WTT	0.67	0.92	−0.6	2.03	2.63	−1.8
77	5152	0.99	17	2.5E+02	0.60	48	0.034	17	9	WTT	0.49	0.80	−0.9	2.63	2.32	
81	4836	1.06	7	2.1E+04	0.60	2	0.028	22	19	WTT	0.54	0.87	−0.6	2.40	2.44	−1.1
83	4150	2.09	8	8.6E+02	0.42	31	0.017	22	6	CTT	0.75	1.17	−0.8	2.10	2.19	−1.7
87	4836	1.61	0.1	2.0E+02	0.60	90	0.051	0	18	CTT	0.56	0.89	−0.9	1.59	1.69	−1.9
89	3999	1.68	4	2.7E+03	0.60	40	0.039	21	12	WTT	1.03	1.19	−0.7	2.17	2.07	−1.4
93	6397	1.69	10	1.6E+03	0.38	61	0.015	9	12	YMS	0.09	0.50	−0.8	2.28	2.06	
99	4775	1.31	25	1.4E+02	1.49	0	0.006	33	19	WTT	0.36	0.84	−0.4	2.52	2.37	
109	6383	1.11	61	1.2E+02	0.46	21	0.007	19	2	CTT	0.06	0.57	−0.9	2.03	1.89	−3.3
110	6653	0.75	13	1.2E+04	0.28	2	0.137	15	11	CTT	0.01	0.45	−0.8	1.83	1.69	
111	5673	1.31	25	2.5E+04	0.30	52	0.038	12	10	CTT	0.17	0.64	−1.0	2.77	2.29	−2.0
115	5636	0.78	1	4.1E+03	0.25	38	0.024	14	8	CTT	0.16	0.66	−0.6	2.75	2.14	−2.1
116	5130	1.06	2	7.5E+03	0.21	0	0.011	18	6	WTT	0.31	0.80	−0.8	1.75	1.71	−1.7
118	6548	1.10	54	9.1E+01	0.42	0	0.028	19	2	CTT	0.05	0.49	−0.9	2.09	1.50	
119	6653	0.73	3	6.1E+05	0.34	72	0.084	5	22	YMS	0.04	0.47	−0.6	2.81	1.23	−3.3
138	2958	13.97	227	5.4E+02	2.53	81	0.102	13	16	WTT		1.70	−0.4	2.55	3.14	−1.0
145	4291	1.49	2	1.4E+02	1.62	0	0.001	29	32	YMS		1.23	0.0	1.97	1.56	−1.7
156	5834	1.51	3	1.5E+02	1.20	2	0.013	24	31	CTT	0.18	0.64	−0.2	1.92	1.29	

Note: In the 'type' column WTT is used to denote weak TTs, PTT, post TTs and YMS, young main-sequence stars.

by assuming those generic relations. The same kind of result was found concerning the radius of the star. We evaluated the theoretical R_s by means of the relations between the spectral type and the stellar radius provided by Straizys & Kuriliene (1981) for main-sequence stars. The values obtained with the SED calculations are slightly higher than the theoretical ones, but still in a good correlation, considering that the radius of the TTs is not accurately derived from the evolutionary tracks. It should be noted that $R_s \sim 15\ R_\odot$ found for PDS138 is unusual, but consistent with its M6III spectral type.

Table 2 gives the best-fitting model parameters: T_s, R_s in terms of $R_\odot$, R_d and R_e in au, optical depth τ (at $\lambda = 1$ μm), disc inclination angle in degrees and the gof given in terms of χ^2. The flux contribution fraction of the circumstellar components, indicated by F_d (S_d/S_{total}) and F_e (S_e/S_{total}), are also given in Table 2.

As examples we show in Fig. 3 the SEDs of PDS039 and PDS054. Different curves are used to indicate the contribution of the star, the disc and the dust envelope. A qualitative analysis of the different curves shows that the near- and mid-IR and millimetre data are mainly fitted by the disc contribution, and the far-IR data is fitted mainly by the envelope emission.

Fig. 3 illustrates the role of of the submillimetre/millimetre observations to probe the properties of the circumstellar structure. These measurements are important to constrain the size of the disc/envelope (see the example of PDS039). For most of our sample, however, the lack of millimetre data does not affect the estimation of S_e and S_d, as can be seen in the PDS054 plot.

4 CLASSIFICATION

The spectroscopic criteria for pre-main-sequence low-mass star classification proposed by Martín (1997) and Martín et al. (1998) were applied to our sample by comparing the equivalent width of Hα ($W_{H\alpha}$) and lithium (W_{Li}) lines with the effective temperature.

In this analysis, we used the stellar temperatures listed in Table 2, adopting a mean error of 150 K. As described in Section 3.4, this is the maximum deviation between T_{eff} and the temperature obtained with the SED fitting calculations (T_s).

By assuming a criterion that considers the Hα dependence on spectral type, we investigated the possible occurrence of CTTs in the sample (Section 4.1). The indication of stellar age was obtained by comparing W_{Li} with the adopted limits of T_{eff} and lithium abundances for TTs (Section 4.2). In order to test the obtained classification, the optical and X-ray properties of the sample were also analysed and compared with the results of the spectroscopic criteria (Sections 4.3 and 4.4, respectively).

4.1 Classical T Tauri stars

In the first selection, the sample was extracted from PDS on the basis of $W_{H\alpha} < 10$ Å, but this does not necessarily imply that the stars are actually WTTs. A definitive distinction between CTTs and WTTs needs additional criteria depending on ultraviolet (UV) and near-IR excesses and the presence of forbidden emission lines (Strom et al. 1993). Most of the PDS spectra covers the 650–675 nm range, but

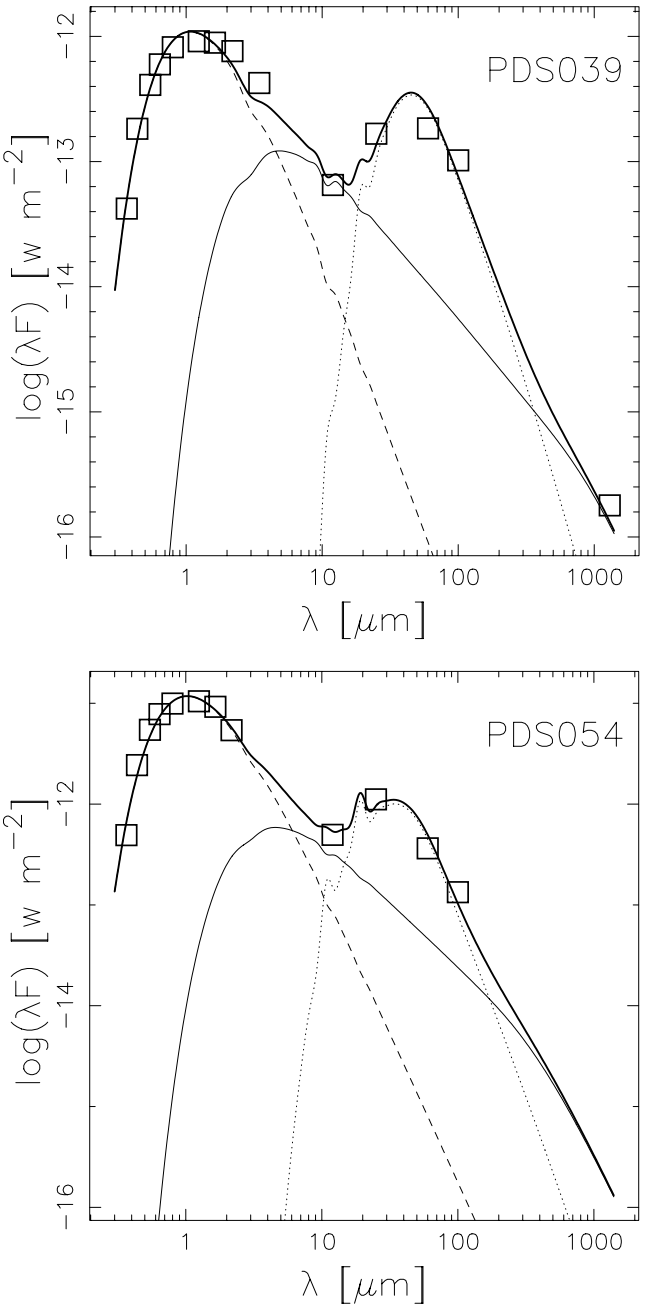

Figure 3. Examples of the fitted SED for two stars of the sample. The continuous bold line is the resulting total emission and different lines are used to show the individual contribution from the star (dashed line), the disc (solid line) and the envelope (dotted line). The observational data are represented by open squares.

some of them reach the 630-nm region, where the [O III] forbidden line occurs. In the case of our sample, six stars have these spectra but only one (PDS115) shows the presence of the [O III] emission line. An inspection of the SED in the lower-wavelength region indicates that none of the stars seems to show UV excess. Among the 10 stars with available near-IR data, *K*-band excess was verified only for PDS039, PDS053 and PDS110. The lack of these information for the whole sample led us to adopt a criterion from Martín et al. (1998). They suggest that Hα emission can vary depending on the spectral type, considering as CTTs K7 (and earlier) type stars showing $W_{\mathrm{H}\alpha}$ larger than 5 and 10 Å for M0–M2 and 20 Å for spectral type later than M2. Following this criterion, the eight earlier-type stars having $5 < W_{\mathrm{H}\alpha} < 10$ Å were classified as CTTs.

PDS109 and 111 show a variable Hα line and were also considered CTTs. This variability was confirmed in a set of spectra obtained for each star at least in three different observational runs. In the case of the remaining stars no Hα line variability was found.

4.2 Lithium versus effective temperature

The lithium measurements were used to estimate the evolutionary status of the sample through the analysis of the diagram of W_{Li} against T_{eff}, where different symbols were used to indicate CTTs (open triangles) and the other objects (filled triangles). This diagram is shown in Fig. 4, where the dashed line represents the cut-off at $T_{\mathrm{limit}} = 5250$ K for TTs. This line also indicates the Li isoabundance $N(\mathrm{Li}) = 2.8$ adopted as a minimum abundance for TTs (Martín 1997). The region above this line is considered to be the expected *locus* of WTT. The position of members of young open clusters is below the dotted line, while the region of post T Tauri stars (PTT) is in the right-hand side of the diagram (below the dashed line and above the dotted one).

We note, in the W_{Li} versus T_{eff} plot, that most of the CTTs falls in the region of low-mass members of young open clusters. The small values of W_{Li} are not related to the age in this case, but are probably a result of veiling effects, which fill the absorption spectrum of CTTs. The remaining four stars in this part of the diagram were classified as YMS and the other two stars falling in the PTT region are considered to be post TT or objects in the transition WTT/PTT. Column 11 in Table 2 gives the classification established from Fig. 4, indicating that only 41 per cent of the sample was classified as WTT.

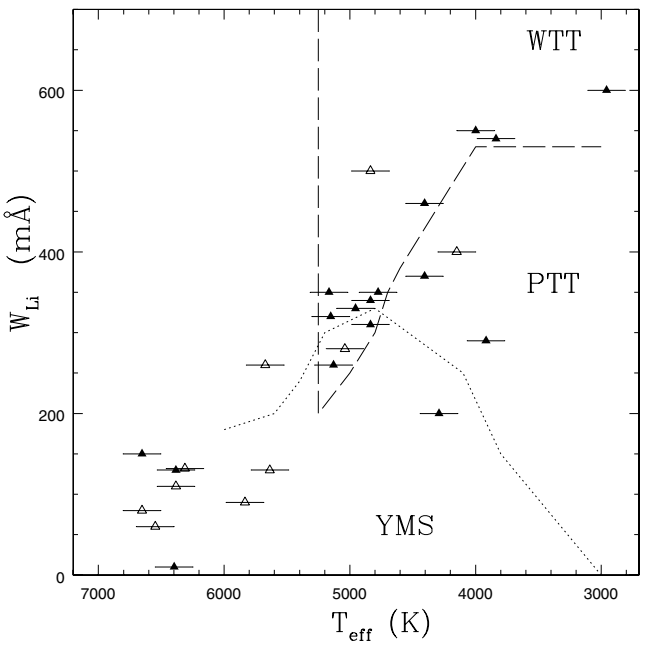

Figure 4. The equivalent width of the Li I line as a function of effective temperature for the programme stars (CTTs are represented by open triangles). Error bars denote the expected difference between the parameter obtained with the SED fit (filled triangles) and the T_{eff} estimated from the spectral type. The dashed line indicates the cut-off proposed by Martín (1997) to separate weak TTs and post TTs, defined by the limits adopted for TTs ($T_{\mathrm{eff}} < 5250$ K and $\log N(\mathrm{Li}) > 2.8$). The position of members of young stellar clusters is below the dotted line.

4.3 Optical colours

The observed *UBV* magnitudes were dereddened using the $(V-I)$ colour index, the spectral types and the intrinsic colours versus spectral-type relation given by Bessel & Brett (1988). The $U-B$ and $B-V$ colours corrected for extinction are listed in Table 2, where it can be noted that most of the CTT and YMS objects are concentrated in the range $U-B<0.2$ and $B-V<0.7$. The only exceptions are PDS039, PDS083 and PDS087 that have lower temperatures among the CTTs. These stars have colours similar to those of WTTs and PTTs, which are mostly $U-B>0.3$ and $B-V>0.8$.

A comparison with Hα shows a good correlation (low $U-B$ and $B-V$ values correspond to low $W_{\mathrm{H}\alpha}$) only for CTTs. The remaining objects have scattered $W_{\mathrm{H}\alpha}$ values for the whole range of colours.

4.4 X-ray emission

The *ROSAT* catalogues were searched for X-ray emitters associated with the programme stars, which resulted in 18 sources (nine WTTs, six CTTs, one PTT and two YMS). The emission could be estimated using the correspondence between count rate and X-ray flux, given by the mean value 9×10^{10} count erg^{-1} cm^2, the energy factor conversion adopted from Neuhäuser et al. (1995b). The obtained X-ray-to-optical flux ratios $\log(f_{\mathrm{X}}/f_V)$, shown in Table 2, were compared with those of the new WTTs in the Chamaeleon star-forming region (Cha) studied by Alcalá et al. (1997).

Following Sterzik et al. (1995) we verified the distribution of $\log(f_{\mathrm{X}}/f_V)$ as a function of visual magnitudes, displayed in Fig. 5. Most of the programme stars are in agreement with the trend shown by the Cha WTTs sample. The distribution is also similar to that found for the TT sample studied by Sterzik et al. (1995), which shows $\log(f_{\mathrm{X}}/f_V)$ in the range of -2.5 to -0.5 for magnitudes $V=10$–15. As expected, PDS119 and PDS145 (YMS) have X-ray emission below the TT level. On the other hand, PDS39 (WTT), PDS051 and PDS109 (CTTs) are quite coincident with the limit line of $f_{\mathrm{X}}=10^{-13}$ erg cm^{-2} s^{-1} shown in Fig. 5, which represents the sensitivity of the *ROSAT* All-sky Survey used by Sterzik et al. (1995). The emission of these three stars is also below the expected TT X-ray flux.

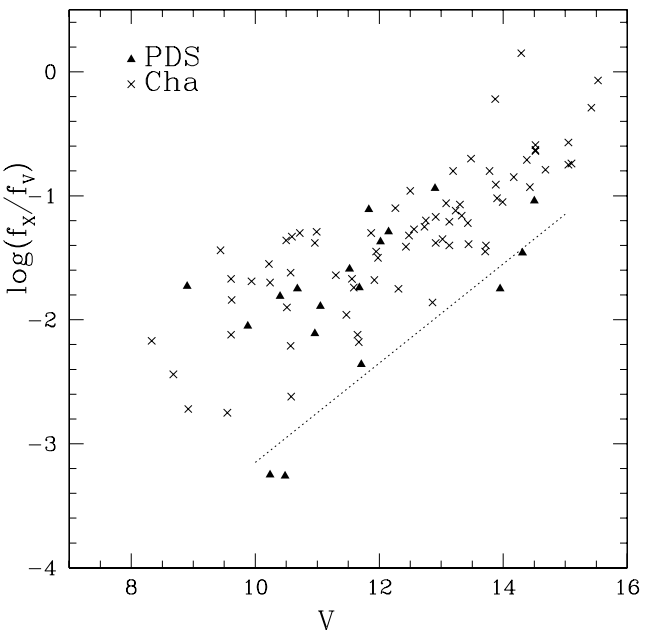

Figure 5. The comparison of the X-ray properties of the programme stars and the Chamaeleon WTT sample studied by Alcalá et al. (1997). The flux ratio $\log(f_{\mathrm{X}}/f_V)$ is plotted against the visual magnitude *V*. Most of the PDS objects follow the trend showed by the Cha sample, excepting PDS109 and PDS119 that are below the expected distribution of TTs. The dotted line indicates the sensitivity of the *ROSAT* survey used by Sterzik et al. (1995).

There is a good agreement of the f_{X}/f_V ratio found for the objects spectroscopically classified as WTT, but the lack of data for the entire sample does not allow us to analyse conclusively the X-ray properties of the objects.

5 INFRARED EXCESS ANALYSIS

The IR excess was computed in three different ways. First we analyse the near-IR spectral index defined by WLY89 and revised by André & Montmerle (1994). We also discuss the IR contribution to the total emitted flux by evaluating the fraction of emission corresponding to each circumstellar component (disc and envelope) as described in Section 3.4. Finally, the far-IR excess is discussed as a function of *IRAS* fluxes by comparing the position of the objects with the distribution of YSOs in a colour–colour diagram defined by Weintraub (1990).

5.1 Spectral index

In this work we assume the scenario for the evolution of YSO, from Class 0 to Class III. The suggestion for an evolutive sequence is based on the spectral index a_{IR} (the SED slope) inspected in the near-IR range. Class III objects have little or no IR excess and show steeper inclination of the SED, corresponding to later epochs of the pre-main-sequence phase, which could be 'naked' TTs or even post TTs. As proposed by André & Montmerle (1994) we adopted $a_{\mathrm{IR}}<-1.5$ to distinguish Class III from Class II objects.

The spectral indices of the sample were estimated in the 1.0–10-μm range by using the synthetic SED curve, since near-IR data is not available for the entire sample. The mean values of a_{IR} are displayed in Table 2 and the distribution of these values is shown in Fig. 6. Most of the programme stars have $-1.0<a_{\mathrm{IR}}<-0.2$, which means that they are Class II objects. Only two stars are out of this range: PDS054 ($a_{\mathrm{IR}}=-1.3$) corresponds to a transition between Class II and Class III, and PDS145 ($a_{\mathrm{IR}}=0$) is in the Class I/Class II transition. This result indicates that no object of the sample could be considered 'naked' TT, since they do not show a steep SED in the near-IR region.

5.2 Computed circumstellar emission

The objects were analysed as a function of their circumstellar contribution (S_{d} and S_{e}) compared with the total emission (S_{total}). The cases where the circumstellar emission is comparable to the stellar contribution ($S_{\mathrm{s}}\sim S_{\mathrm{d}}+S_{\mathrm{e}}$) may be interpreted as the phase when the star becomes visible but is still surrounded by a significant amount of dust. These objects are considered in the transition Class I/Class II and they show a roughly flat SED ($a_{\mathrm{IR}}\sim0$), but some of them can have a depression in the near-IR wavelength range, showing a double-peaked SED.

The evolved objects, which could be interpreted as the post TT phase, should not present an important IR excess ($S_{\mathrm{s}}\gg S_{\mathrm{d}}+S_{\mathrm{e}}$) and the expected SEDs should be similar to reddened blackbody emission ($a_{\mathrm{IR}}<-1.5$).

In order to confirm the evolutionary status of the stars, the fraction of flux emitted by the circumstellar components is compared with

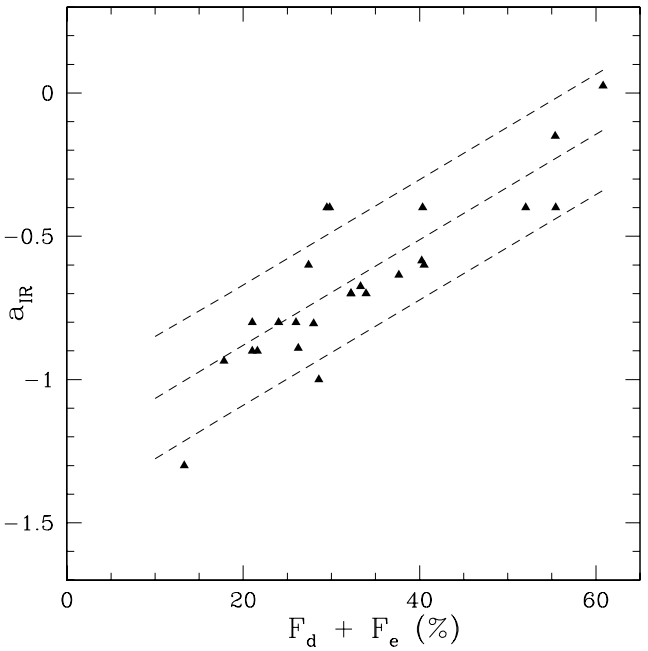

Figure 6. The spectral indices, estimated in the 1.0–10-μm range, as a function of the circumstellar contribution in the total flux ($F_e + F_d$). The full line indicates the linear regression for the PDS sample, and dashed lines are used to indicate a 2σ deviation.

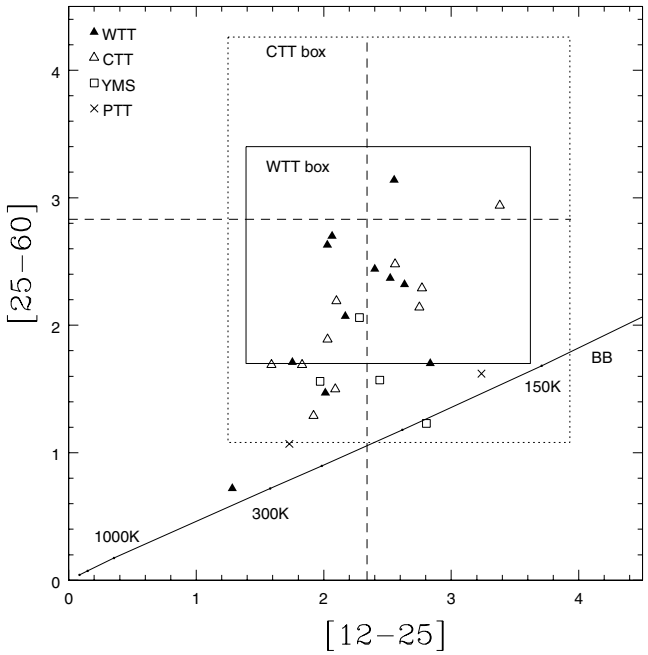

Figure 7. *IRAS* colours diagram, showing the expected *locus* for T Tauri stars (CTTs, dotted lines and WTTs, solid lines), following Weintraub (1990). Dashed lines indicate the regions corresponding to a falling spectrum ([12–25] < 2.34 or [25–60] < 2.83), and rising spectrum region (above these values). The warm sources are found in the lower left-hand side, and very cold material in the upper right-hand side. The blackbody colour–colour is indicated by the solid line covering a range of temperatures.

the above discussed classes (see Fig. 6). We considered the least-squares method and used a straight-line model to fit the data points in this plot. A good correlation is verified, as indicated by the fitted line: $a_{IR} = -1.25 + 0.018(F_d + F_e)$, where the mean deviation is $\sigma = 0.11$.

The disc and envelope contribute with a small fraction of the total emission ($S_d + S_e < 0.18 S_{total}$) in the case of PDS054 (PTT) and PDS087 (CTT). Most of the stars (76 per cent of the sample) have moderate circumstellar contributions (∼20–40 per cent of the total flux). Four stars: PDS035 (CTT), PDS099 (WTT), PDS145 (YMS) and PDS156 (CTT) have circumstellar emission greater than the stellar emission ($S_d + S_e > 0.5 S_{total}$). This means that the amount of circumstellar emission is not consistent with the classic evolutive scenario, where a higher circumstellar contribution is expected for CTTs as compared with WTTs or YMS objects.

5.3 *IRAS* colours

The far-IR colours were calculated using the index colour definition $[\lambda_i - \lambda_j] = -2.5 \log(f_{0j} F_{\lambda_i} / f_{0i} F_{\lambda_j})$, where F_λ are the *IRAS* fluxes and $f_0 = 28.3$, 6.73 and 1.19 Jy for $\lambda = 12$, 25 and 60 μm, respectively.

The obtained *IRAS* colours are presented in Table 2. Fig. 7 shows the [12–25] versus [25–60] diagram, displaying the *locus* expected for WTTs, delimited by the solid lines box and the region of CTTs (dotted lines box). Most of the objects have a far-IR excess similar to the WTTs and lie well above the indicated blackbody colour–colour line, which implies the presence of cold circumstellar material. The region corresponding to warm sources (lower left-hand side of the diagram) is separated from the region of very cold material (upper right-hand side) by dashed lines, which also represent the limits for a rising spectrum ([12–25] >2.34 or [25–60] > 2.83) and a falling spectrum (below these values).

A good correlation between a_{IR} and [25–60] is verified, which is related to the predominant SED shape of our sample in these bands. Even if the SED shows a double peak, the far-IR slope is systematically decreasing, as well as the near-IR spectral indices. The same cannot be said concerning the slope in the mid-IR region by considering that for the [12–25] colour the sources are scattered in both regions of rising and falling spectrum.

The spatial distribution of the sources was investigated in order to verify whether there is any correlation of *IRAS* excess and proximity to molecular clouds. Only eight stars are isolated from clouds. The analysis of the amount of circumstellar emission for the 14 objects, which are close to clouds, shows that 21 per cent of them have low circumstellar emission and 58 per cent have moderate $S_d + S_e$ values. Only four objects have high *IRAS* excess (>45 per cent of the total flux), but it does not seem that it could be caused by background contamination, considering that poor quality data points were not used in the calculations, which guarantees circumstellar origin of the excess. This is also confirmed by the *IRAS* colours of our sample, which is mainly coincident with the typical WTTs colours defined by Weintraub (1990).

6 CONCLUSIONS

A simple three-component model was used to explain the circumstellar structure of YSOs by a χ^2 fitting of the observed SED. The individual contribution to the total luminosity of the system could be evaluated and compared with other indicators of the evolutive status of a selected PDS sample showing $W_{H\alpha} < 10$ Å, which in principle do not show accretion activity.

The adopted spectroscopic criteria indicate that a significant part (37 per cent) of our sample should be classified as CTT and 22 per

cent seems to be more evolved than TTs: four stars are considered YMS and two are PTT. The classification based on the spectroscopic Li versus $T_{\rm eff}$ criterion was verified by means of the analysis of optical, IR and X-ray properties. In a comparison of the $B-V$ and $U-B$ colours WTT and PTT are clearly distinguished from CTT and YMS, owing to the difference in $T_{\rm eff}$, which is higher for these two groups in the sample. The far-IR excess is similar for both WTT and CTT categories, but a concentration of objects in the region corresponding to a falling spectrum in the far-IR range ([25–60] < 2.83) is noted.

It is more complicated to distinguish the groups based on the X-ray emission, given the lack of data for the entire sample. Only 18 objects were detected as X-ray sources: nine are WTTs and six are CTTs. However, the results are similar to those found in the optical colours analysis and a good agreement with the X-ray-to-optical flux ratio expected for TTs is found (except for PDS039, PDS051 and PDS109). An expected non-correlation of f_X/f_V is found for the YMSs.

All the objects classified as WTTs belong to the Class II category. This fact is in agreement with the discussion presented by André & Montmerle (1994) in a comparison between the near-IR and Hα classification. They found that $a_{\rm IR} < -1.5$ (Class III) always implies $W_{\rm H\alpha} < 10$ Å, but the contrary is not valid, since about half of the WTT sample studied by them shows $a_{\rm IR} > -1.5$ (Class II).

We have shown that the circumstellar contribution ($F_{\rm d}+F_{\rm e}$) is well correlated with $a_{\rm IR}$. The mean straight line obtained by linear regression is slightly less steeped than expected theoretically: the $a_{\rm IR}$ axis is intercepted at $a_{\rm IR}\sim -1.3$, and should be $a_{\rm IR} < -1.5$. By considering that PDS objects were originally selected owing to their IR excess (at least in the *IRAS* range), the fact that they are not 'naked TTs' is not surprising. However, the analysis of the circumstellar emission, provided by the estimation of the disc and envelope contribution to the total flux, indicates that the amount of IR excess is not large in this sample. Most of the objects have about a 30 per cent circumstellar contribution in the total emitted flux and two stars (PDS054 and PDS087) have very little contribution from the disc and/or the envelope ($S_{\rm e}+S_{\rm d} < 0.2 S_{\rm total}$).

On the other hand, PDS035 and PDS156 show $S_{\rm e}+S_{\rm d} > 0.5 S_{\rm total}$, as expected for CTTs, but one YMS (PDS145), and one WTT (PDS099) show the same level of excess, which is surprising. The large amounts of dust emission for these four objects are in good agreement with the high values of near-IR spectral index $a_{\rm IR}$ presented by them. In spite of this, an evolutionary sequence could not be inferred from the circumstellar contribution.

Some inconsistencies in a coherent classification of the studied sample might arise from different geometries and sizes of the assumed dust distribution around each object. For example, a disrupted disc could produce a double-peak in near- and far-IR.

The SED of the sample suggests that the dust structure could correspond to a breakup of the disc, with an inner part (hotter region) where the dust disappears faster than in the outer part of the disc. This is indicated by the decreasing near- to far-IR dust emission, often shown by a dip in the 10-μm region, which could be interpreted by a cavity in the inner part of the disc. As a follow-up of this work, we are improving the SED calculations to adopt a variable disc geometry, in order to introduce the presence of warps, localized clumps or radial gaps. It has been suggested that disruption of the disc and the dispersal of the protostellar dust might precede planet formation. The main conclusion of the present work shows that WTTs without accretion indices (as indicated by the low $W_{\rm H\alpha}$), and still having considerable amounts of circumstellar dust (Class II objects, $F_{\rm d}+F_{\rm e}\sim 30$ per cent), are good candidates for having more evolved discs, a condition to form the substructures expected to be found in protoplanetary discs.

ACKNOWLEDGMENTS

This paper is based on observations collected at *Observatório do Pico dos Dias*, LNA/MCT, Brazil. We thank J.R.D. Lépine, S.H.P. Alencar, D. Ellison and L.H.J. Monteiro Filho for some helpful suggestions and an anonymous referee for useful comments, which have improved the presentation of the paper. This work was partially supported by grants CNPq No 300267/92-4 (JG-H) and UNIP No 031521437/0 (AH).

REFERENCES

Adams F.C., Shu F.H., 1986, ApJ, 308, 836
Adams F.C., Lada C., Shu F.H., 1987, ApJ, 312, 788
Alcalá J.M., Krautter J., Schmitt J.H.M.M., Covino E., Wichmann R., Mundt R., 1995, A&AS, 114, 109
Alcalá J.M., Krautter J., Covino E., Neuhäuser R., Schmitt J.H.M.M., Wichmann R., 1997, A&A, 319, 184
André Ph., Montmerle T., 1994, ApJ, 420, 837
André Ph., Ward-Thompson D., Barsony M., 1993, ApJ, 406, 122
Appenzeller I., Mundt R., 1989, ARA&A, 1, 291
Beichman C.A., 1986, in Israel F.P., ed. Light on Dark Matter. Reidel, Dordrecht, p. 279
Bessel M., Brett J.M., 1988, PASP, 100, 1134
Bouvier J., Bertout C., 1992, A&A, 263, 113
Briceño C., Hartmann L.W., Stauffer J., Gagné M., Stern R.A., Caillaut J.-P., 1997, AJ, 113, 740
Calvet N., Hartmann L., Kenyon S.J., Whitney B.A., 1994, ApJ, 434, 330
Chiang E.I., Goldreich P., 1997, ApJ, 490, 368
Chiang E.I., Goldreich P., 1999, ApJ, 519, 279
Chiang E.I., Joung M.K., Creech-Eakman C. QI., Kesseler J.E., Blake G.A., van Dishoeck E.F., 2001, ApJ, 547, 1077
D'Alessio P., Calvet N., Hartman L., Lizano S., Cantó J., 1999, ApJ, 527, 893
de Jager C., Nieuwenhuijzen H., 1987, A&A, 177, 217
Désert F.-X., Boulanger F., Puget J.L., 1990, A&A, 237, 215
Epchtein N., Le Bertre T., Lépine J.R.D., 1990, A&A, 227, 82
Gregorio-Hetem J., Sanzovo G.C., Lépine J.R.D., 1988, A&AS, 76, 347
Gregorio-Hetem J., Lépine J.R.D., Ortiz R.P., 1990, Rev. Mexicana Astron. Astrof., 21, 356
Gregorio-Hetem J., Lépine J.R.D., Ortiz R.P., 1991, in Falgarone, et al. eds, Proc. IAU Symp. 147, Fragmentation of Molecular Clouds and Star Formation. Kluwer, Dordrecht, p. 427
Gregorio-Hetem J., Lépine J.R.D., Quast G.R., Torres C.A.O., de la Reza R., 1992, AJ, 103, 549 (PDS I)
Harris S., Clegg P., Hughes J., 1988, MNRAS, 235, 441
Henning Th., Pfau W., Zinnecker H., Prusti T., 1993, A&A, 276, 129
Herbig G.H., Bell K.R., 1988, Lick Obs. Bull. No 1111 (HBC)
Hetem A., Jr, Gregorio-Hetem J., Lépine J.R.D., 1994, in Ferlet R., Vidal-Madjar A., eds, Circumstellar Dust Discs and Planet Formation. Éditions Frontières, Paris, p. 369
Kenyon S.J., Hartmann L.W., 1987, ApJ, 323, 714
Lada C.J., Wilking B.A., 1984, ApJ, 287, 610
Martín E.L., 1997, A&A, 321, 492
Martín E.L., Montmerle T., Gregorio-Hetem J., Casanova S., 1998, MNRAS, 300, 733
Natta A., 1993, ApJ, 412, 761
Neuhäuser R., Sterzik M., Torres G., Martín E.L., 1995a, A&A, 299, L13
Neuhäuser R., Sterzik M.F., Schmitt J.H.M.M., Whichmann R., Krautter J., 1995b, A&A, 297, 391
Ossenkopf V., 1993, A&A, 280, 617
Press W.H., Teukolsky S.A., Vetterling W.T., Flannery B.P., 1992, Numerical Recipes. Cambridge Univ. Press, Cambridge

Rowan-Robinson M., 1980, ApJS, 44, 403
Rowan-Robinson M., 1986, MNRAS, 219, 737
Sterzik M.F., Alcalá J.M., Neuhäuser R., Schimitt J.H.M.M., 1995, A&A, 297, 418
Straizys V., Kuriliene G., 1981, Ap&SS, 80, 353
Strom S.E., Edwards S., Strutskie M.F., 1993, in Levy E.H., Matthews M.S., Protostars and Planets III. Univ. Arizona Press, Tucson
Thamm E., Stinacker J., Henning Th., 1994, A&A, 287, 493
Torres C.A.O., 1998, PhD thesis, CNPq/Observatório Nacional (Brazil)
Torres C.A.O., Quast G.R., de la Reza R., Gregorio-Hetem J., Lépine J.R.D., 1995, AJ, 109, 2146 (PDS II)
Weaver W.B., Jones G., 1992, ApJS, 78, 239
Weintraub D.A., 1990, ApJS, 74, 575
Wilking B.A., Lada C.J., Young E.T., 1989, ApJ, 340, 823 (WLY89)

This paper has been typeset from a TEX/LATEX file prepared by the author.